Supporting Information

Electronic structure modulation of bifunctional oxygen catalysts for rechargeable Zn-air batteries

Jian Yang[a, 1], Le Chang[b, 1], Heng Guo[c], Jiachen Sun[b], Jingyin Xu[b], Yanning Zhang[b], Zhiming Wang[b], Liping Wang[*a], Feng Hao[*a] and Xiaobin Niu[*a]

[a] School of Materials and Energy, University of Electronic Science and Technology of China, Chengdu 610054, China
[b] Institute of Fundamental and Frontier Sciences, University of Electronic Science and Technology of China, Chengdu 610054, China
[c] School of Materials Science and Engineering, Southwest Petroleum University, No. 8, Xindu Road, Xindu District, Chengdu, 610500, China

[*] Corresponding author: lipingwang@uestc.edu.cn; haofeng@uestc.edu.cn; xbniu@uestc.edu.cn;
[1] The authors contributed equally to this work.

1.Experimental Section

***Chemicals**:* Dicyandiamide (DCDA), Ruthenium Chloride ($RuCl_3$), Cobalt chloride hexahydrate ($CoCl_2$•$6H_2O$), Potassium Hydroxide (KOH), Zinc Acetate Dihydrate ($Zn(ac)_2$•H_2O) were purchased from Adamas-beta. Sulfuric acid and ethanol were obtained from Chengdu Kelong Chemicals Co., Ltd. 5% Nafion solution, RuO_2 and 20wt% Pt/C commercial catalysts were originated from Sigma-Aldrich and Johnson Matthey Company, respectively. Carbon cloth was purchased from CeTech CO., Ltd., China.

***Preparation of RuCo/N-CNT**:* The RuCo/N-CNT was prepared by pyrolysis and acid etching. Typically, 1.4 g (6.0 mmol) of $CoCl_2$•$6H_2O$ and 0.125 g (0.6 mmol) of $RuCl_3$ were dissolved in 100 mL deionized water, then 6.0 g of DCDA were added in the above-mentioned solution under magnetic stirring. When the solution was evaporated at 80 ^oC for overnight, as-formed solid were ground and placed in the center of quartz tube, followed by a pyrolysis process in argon atmosphere from room temperature to 550 ^oC for 120 min with the heating rate of 2.5 ^oC/min, then heated to 800 ^oC for 120 min at a rate of 10 ^oC/min. After that, the furnace was cooled to room temperature naturally under Ar flow. The pristine black products were etched by 0.5 M H_2SO_4 for 8h at 80 ^oC with two times, rinsed with deionized water or ethanol several times, and dried at 80 ^oC for 24 h. Thus RuCo/N-CNT catalyst was prepared.

For preparing $RuCoO_x$@Co/N-CNT, 100 mg of RuCo/N-CNT were distributed in the quartz boat and transferred to the center of a tube furnace. In the air atmosphere, the furnace was heated to 250 ^oC for 2h with a heating rate of 2 ^oC/min. Then the $RuCoO_x$@Co/N-CNT catalyst was prepared.

Preparation of Co/N-CNT: The Co/N-CNT was prepared via similar procedure of RuCo/N-CNT except $RuCl_3$. The CoO_x@Co/N-CNT was fabricated from Co/N-CNT by the same procedure as $RuCoO_x$@Co/N-CNT.

Characterization: The morphologies of the samples were conducted using transmission electron microscopy (TEM; Tecnai G2 F30 and Talos F200C field emission transmission electron microscope (FEI, USA) at operating voltages of 300

and 200 kV, respectively.) and field-emission scanning electron microscopy (FESEM; Hitachi SU-8010). Powder X-ray diffraction (XRD) measurements were performed on Bruker D8 Advance diffractometer with CuKa1 radiation (λ=0.15406 nm). X-ray photoelectron spectroscopy (XPS) were measured on an X-ray photoelectron spectrometer (Thermo ESCALAB 250). Raman scattering measurements were performed using a multichannel modular triple Raman system, with confocal microscopy at room temperature and an excitation wavelength of 532 nm. The Brunauer-Emmett-Teller (BET) specific surface area was determined by nitrogen adsorption-desorption isotherm measurements at 77 K (NOVA 2200e), while pore-size distribution was calculated with the supplied Barrett-Joyner-Halenda (BJH) software package. The content of Ru and Co in the catalyst was verified by Inductively coupled plasma (ICP-OES) (Agilent 720).

Electrocatalysis measurements*:* The electrochemical measurements were conducted in a typical three-electrode electrochemical system by using a CHI 760E electrochemical workstation. The glassy carbon electrode (diameter = 5.0 mm) as working electrode, Ag/AgCl (saturated KCl) electrode as reference electrode, Pt wire as counter electrode as well as a rotator were purchased from Pine Instruments (MSR). All the potentials were calibrated to the reversible hydrogen electrode according to the Nernst equation: $E_{RHE}=E_{Ag/AgCl}+0.197+0.0591pH$. The oxygen catalysis performances were measured in the O_2 or N_2 saturated 0.1 M KOH aqueous solution. The cyclic voltammograms (CV) were collected at 50 mV s^{-1} and the linear sweep voltammetry (LSV) curves were obtained at 10 mV s^{-1} from 1.2 V to 0.1 V (vs. RHE).

In the RRDE measurement, the Pt ring electrode was polarized at 1.3 V vs. RHE to oxidize HO_2^- intermediate from the disk electrode. The number of electrons transferred per oxygen molecule (n) and the kinetic current density (j_k) can be extracted

from the Koutecky-Levich (K-L) equation.

$$\frac{1}{j} = \frac{1}{j_k} + \frac{1}{B}\omega^{-1/2}$$

$$B = 0.2nF(D_{O_2})^{2/3}v^{-1/6}C_{O_2}$$

Where F is the Faraday constant (96485 C mol^{-1}), D_{O_2} is the diffusion coefficient of O_2 in 0.1 M KOH (1.9×10^{-5} cm^2 s^{-1}), v is the kinematic viscosity (0.01 cm^2 s^{-1}), and C_{O_2} is the bulk concentration of O_2 in the solution (1.2×10^{-6} mol cm^{-3}). The constant 0.2 is adopted when the rotation speed is expressed in rpm. The n values can also be calculated according to the following equations.

The electron transfer number (n) and percentage of peroxide species (HO_2^-%) are calculated by the following equations:

$$n = 4\frac{|I_d|}{(|I_d| + \frac{I_r}{N})}$$

$$HO_2^-(\%) = 200 \times \frac{I_r}{I_r + N|I_d|}$$

Where I_d is the disk current, I_r is the ring current, and N is the current collection efficiency of the Pt ring, which is determined to be 0.38.

Preparation of working electrode: the catalyst ink was prepared by dispersing 4 mg of catalyst into 960 uL of water-ethanol solution with a volume ratio of 4:1 and 40 uL of 5% Nafion solution. After sonicating treatment for at least 60 min to form a homogeneous ink, 20 uL of as-prepared ink was dropped onto the clear surface of glassy carbon by Eppendoff and dried at room temperature naturally. The catalyst loading on the glassy carbon electrode is about 0.4 mg cm^{-2}.

Zn-air battery assembly and test: The Zn-air batteries were composed of a polished zinc plate with a 0.3 mm thickness as anode, an air electrode as cathode, and 6.0 M KOH with 0.2 M zinc acetate as electrolyte. The air electrode is mainly constituted of gas diffusion layer (GDL) with a catalyst ink layer on the water-facing side. The catalyst loading was 1.0 mg cm^{-2}. When assembling Zn-air battery, the nickel foam was used as current collector attached to the air-facing side of GDL. The galvanostatic discharge (ORR) and discharge-charge (ORR-OER) cycling stability were determined using a LAND testing system. Both the discharge and charge currents and corresponding power densities were normalized to the effective surface areas of the air–cathode electrodes.

2. Computational Details

DFT calculations were performed with the spin-polarized planewave method implemented in the Quantum Espresso package. The Perdew–Burke–Ernzerhof (PBE) functional based on the generalized gradient approximation (GGA) were employed to evaluate the non-local exchange-correlation (xc) energy. In a cubic supercell, the values of 40 and 400 Ry were used as the kinetic energy cutoff for wave functions and charge densities. The current work employs the metallic (6,6) carbon nanotube (CNT). The metal clusters, Co_{13} and $Co_{12}Ru$, with Mackay icosahedral structure, which is commonly found as the lowest-energy motif of free clusters, were selected. The metallic oxide, CoO and Ru-doped CoO nanoparticles, were taken from the 110 surface of CoO surface. The possible positions of the atoms in the complex were fully optimized until the forces were smaller than 0.01 eV $Å^{-1}$ per atom. The first Brillouin zone was sampled at the G point, and the electronic levels were broadened with a

Gaussian smearing of about 0.002 Ry. The self-consistent field calculation has convergence criteria of 10^{-6} Hartree. The spin-polarization calculation was considered throughout the DFT calculation. The adsorption Gibbs free energy of ORR intermediates were calculated following the detailed approach of NØrskov et al. [1-2] and Chang-Yuan et al.[3]

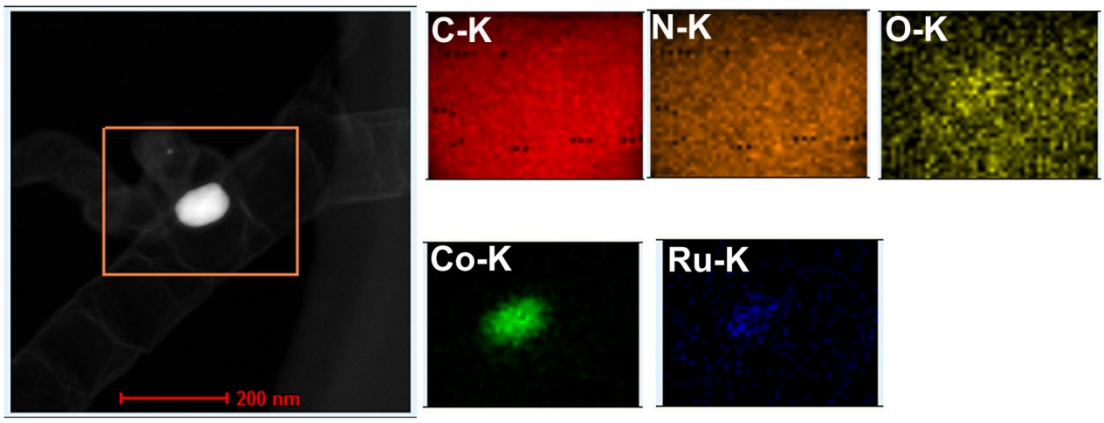

Fig. S1. HAADF-STEM image and elemental mapping of RuCo/N-CNT.

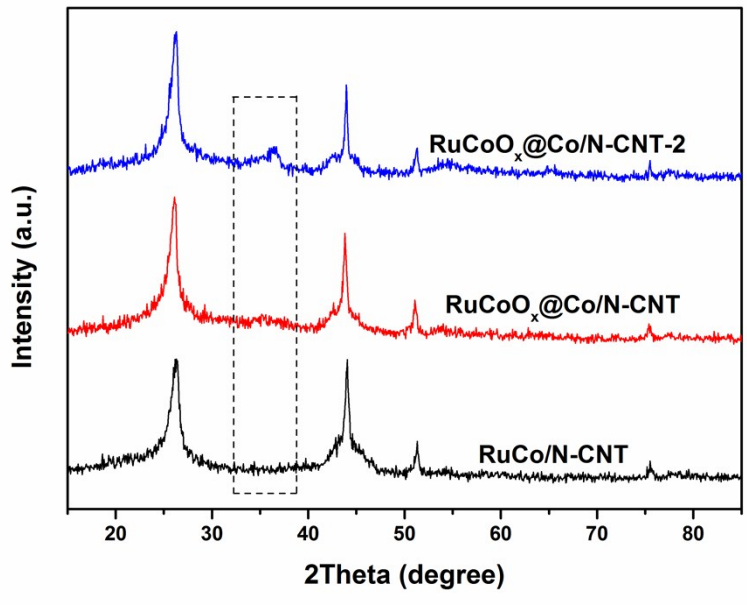

Fig. S2. The XRD patterns of RuCo/N-CNT, RuCoO$_x$@Co/N-CNT, and RuCoO$_x$@Co/N-CNT-2 (prepared by post-oxidation treatment at 350 ^{o}C for 2h in air atmosphere).

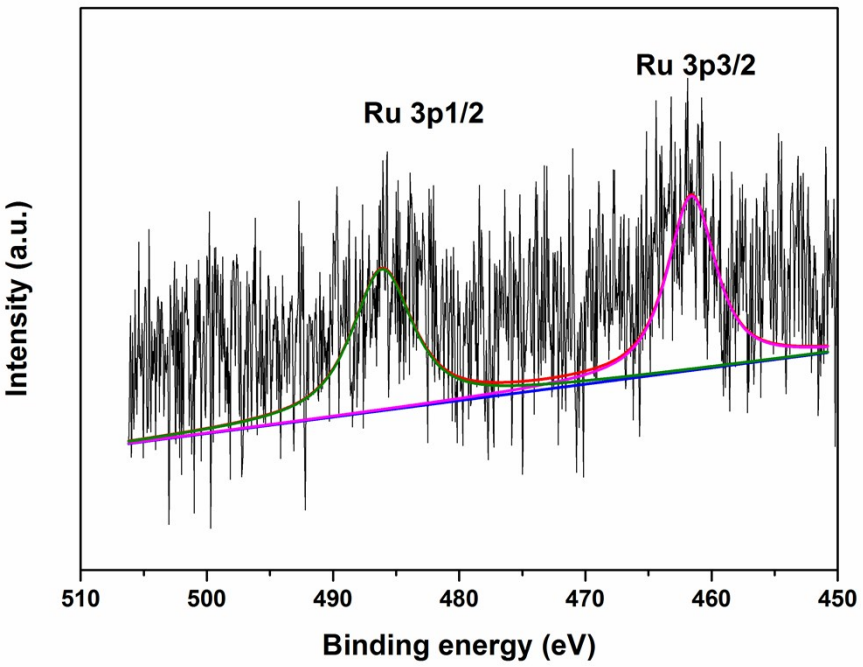

Fig. S3. High-resolution Ru 3p of $RuCoO_x$@Co/N-CNT.

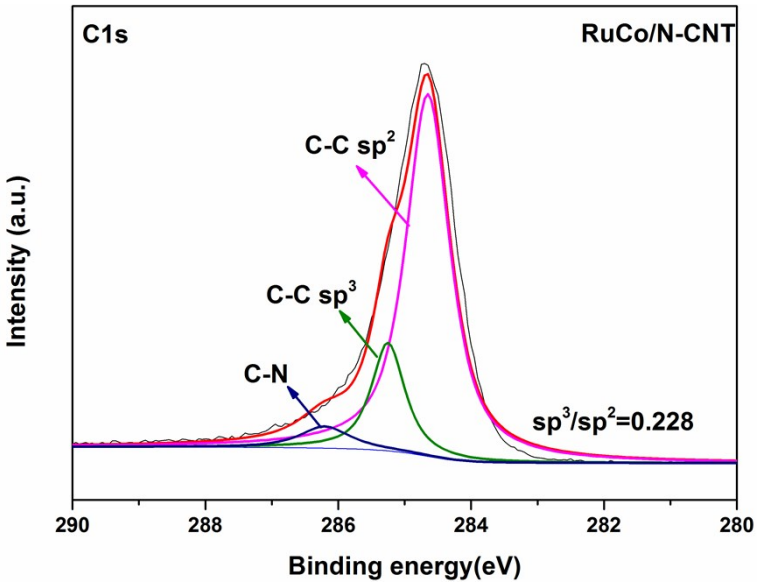

Fig. S4. High-resolution C 1s of RuCo/N-CNT.

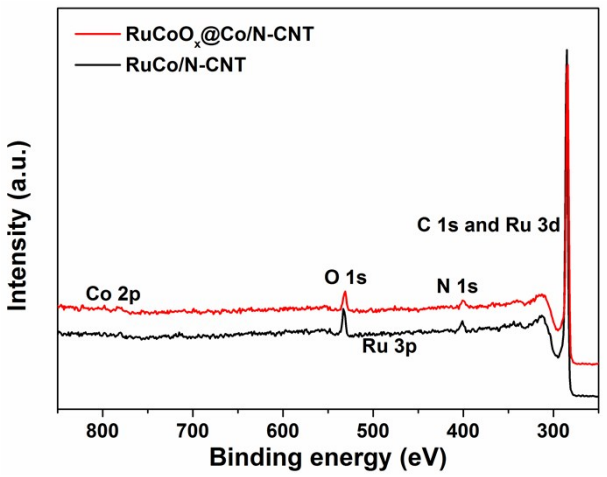

Fig. S5. XPS survey of RuCo/N-CNT and RuCoO$_x$@Co/N-CNT.

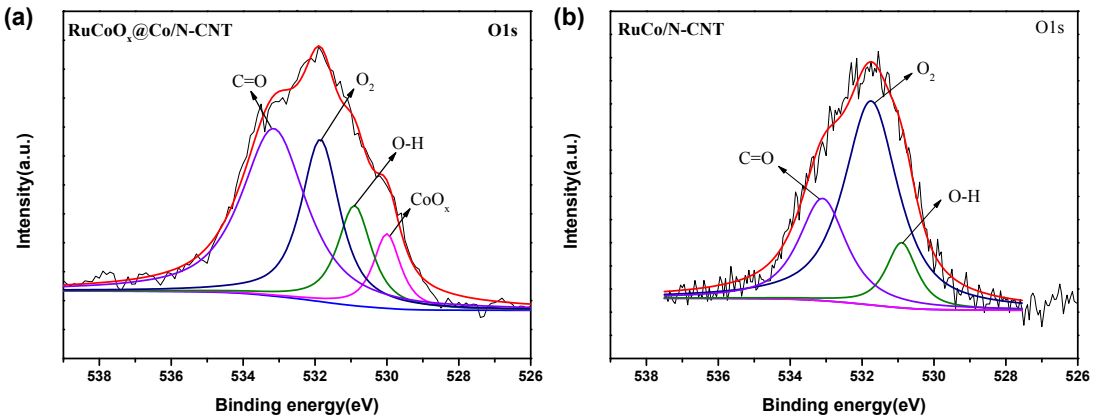

Fig. S6 High-resolution O 1s of $RuCoO_x$@Co/N-CNT (a) and RuCo/N-CNT(b).

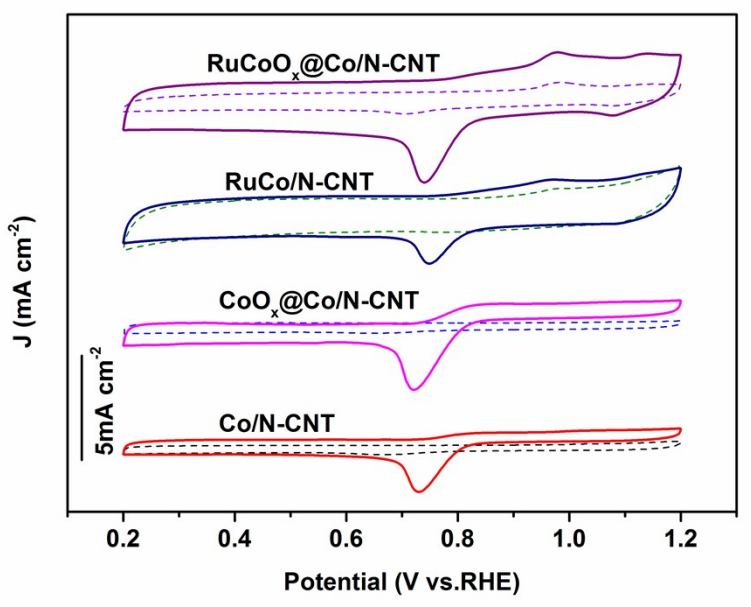

Fig. S7 CV curves of Co/N-CNT, CoO_x@Co/N-CNT, RuCo/N-CNT, and $RuCoO_x$@Co/N-CNT in O_2-saturated (solid line) and N_2-saturated (dotted line) 0.1 M KOH.

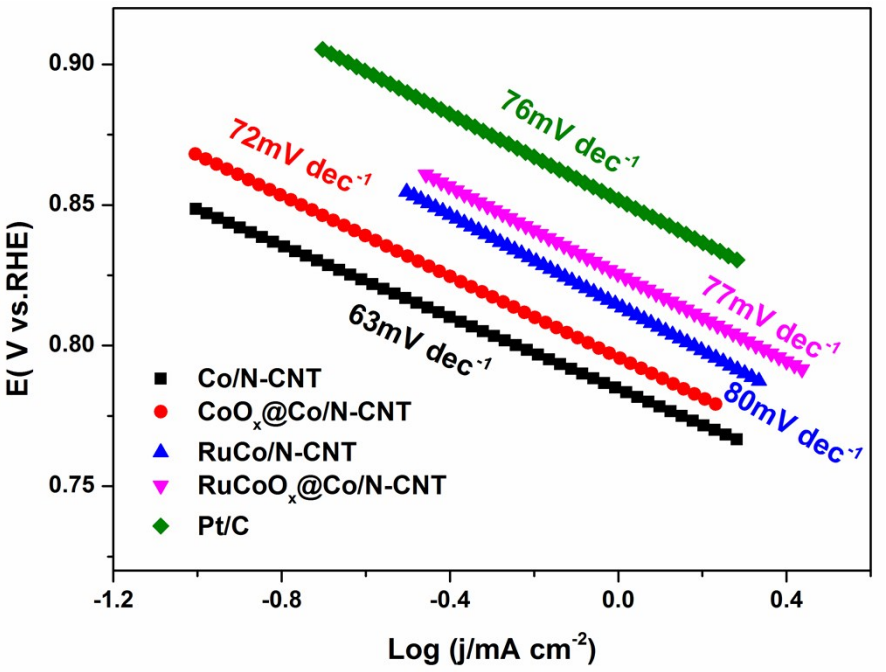

Fig. S8 Tafel slope values at low overpotential regions for ORR based on LSV curves.

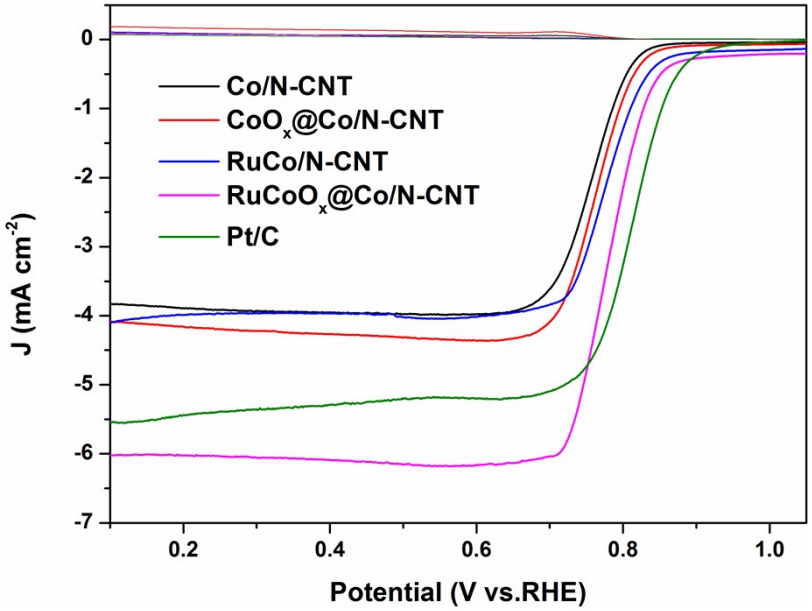

Fig. S9 The i-E curves and LSV curves of ring and disk electrode on the RRDE.

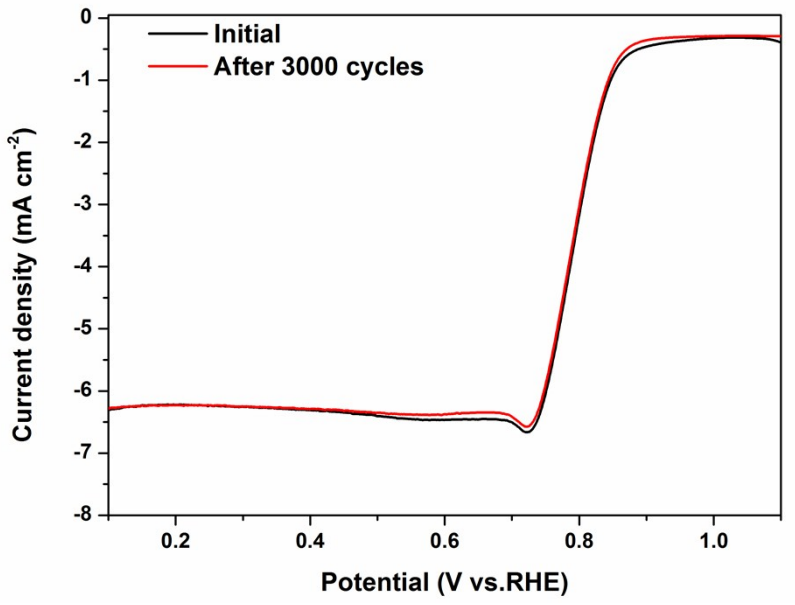

Fig. S10 ORR polarization curves of the commercial $RuCoO_x$@Co/N-CNT before and after 3000 cycles.

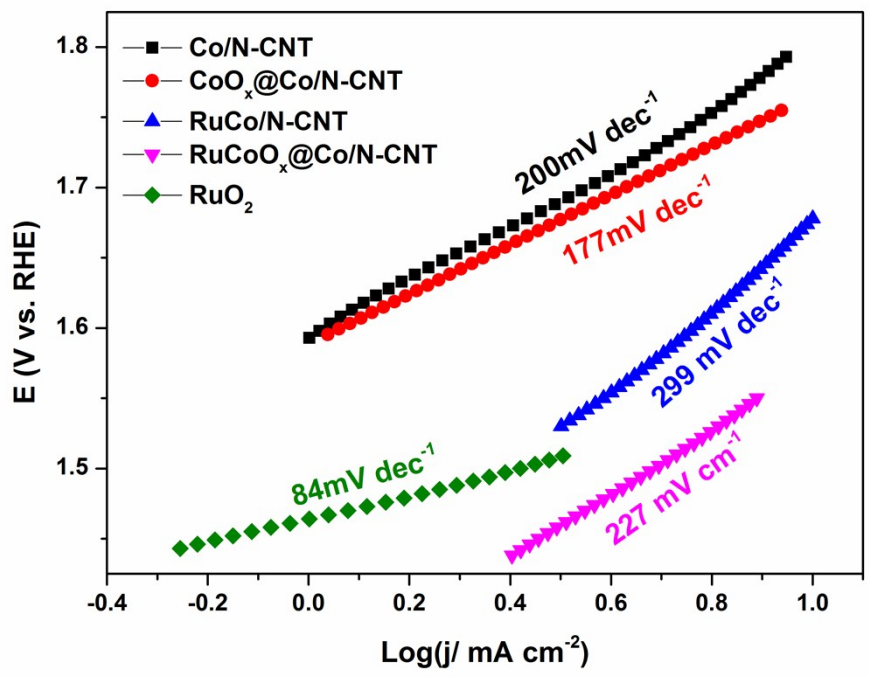

Fig. S11 Tafel slope values at low overpotential regions for OER based on LSV curves.

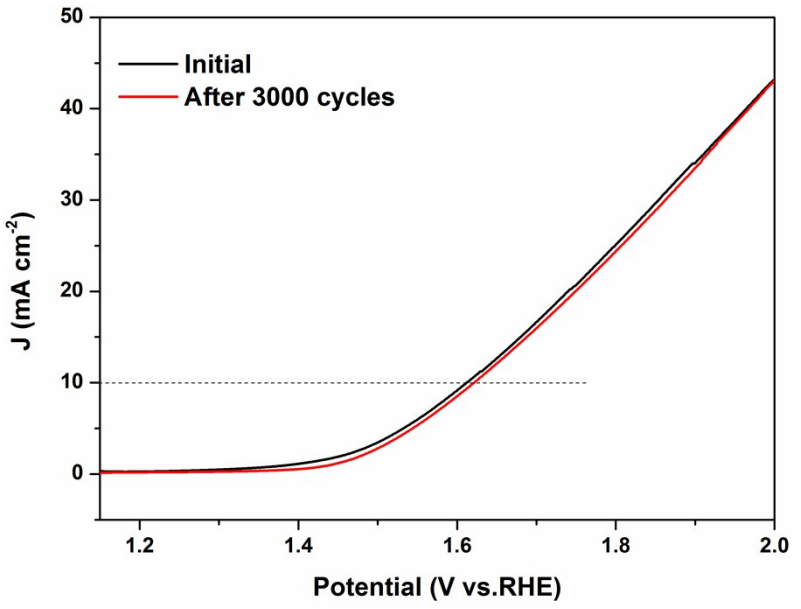

Fig. S12 OER polarization curves of the commercial $RuCoO_x$@Co/N-CNT before and after 3000 cycles

Table S1. The electrocatalytic activities of the recently reported bifunctional catalysts for ORR and OER.

electrocatalysts	E_{onset}/V vs. RHE	$E_{1/2}$/V vs. RHE	E_{OER}/ V (at 10 mA cm^{-2}) vs. RHE	ΔE	Ref.
$RuCoO_x$@Co/N-CNT	0.85	0.79	1.58	0.79	This work
RuCo/N-CNT	0.84	0.79	1.67	0.88	This work
Co/N-CNT	0.80	0.76	1.80	1.04	This work
CoOx@Co/N-CNT	0.82	0.76	1.78	10.2	This work
Pt/C	0.99	0.90	1.90	1.0	[4]
N-GCNT/FeCo-3	/	0.92	1.73	0.81	[3]
3D NCNT array	/	0.81	1.65	0.84	[5]
S, N-Fe/N/C-CNT	/	0.85	1.60	0.75	[6]
NPMC-1000	/	0.85	1.93	1.08	[7]
FeN_x-embedded PNC	0.997	0.86	1.62	0.76	[8]
$(Mg, Co)_3O_4$@NGC	0.925	0.842	1.576	0.73	[9]
Fe@C-NG/NCNTs	0.93	0.84	1.68	0.84	[10]
Co_3O_4/MnO_2/PQ-7	0.95	~0.90	~1.78	0.88	[11]
NiFe@NBCNT	1.03	0.83	~1.44	0.61	[12]
CoP	0.92	0.86	~1.49	0.63	[13]

References

1 J.K. Nørskov, J. Rossmeisl, A. Logadottir, L. Lindqvist, J.R. Kitchin, T. Bligaard and H. Jónsson, J. Phys. Chem. B, 2004, **108**, 17886-17892.

2 F. Calle-Vallejo, J.I. Martinez and J. Rossmeisl, Phys. Chem. Chem. Phys., 2011, **13**, 15639-15643.

3 C.-Y. Su, H. Cheng, W. Li, Z.-Q. Liu, N. Li, Z. Hou, F.-Q. Bai, H.-X. Zhang and T.-Y. Ma, Adv. Energy Mater., 2017, **7**, 1602420.

4 A. Aijaz, J. Masa, C. Rosler, W. Xia, P. Weide, A.J. Botz, R.A. Fischer, W. Schuhmann and M. Muhler, Angew. Chem., Int. Ed., 2016, **55**, 4087-4091.

5 Z. Li, M. Shao, Q. Yang, Y. Tang, M. Wei, D.G. Evans and X. Duan, Nano Energy, 2017, **37**, 98-107.

6 P. Chen, T. Zhou, L. Xing, K. Xu, Y. Tong, H. Xie, L. Zhang, W. Yan, W. Chu, C. Wu and Y. Xie, Angew. Chem., Int. Ed., 2017, **56**, 610-614.

7 J. Zhang, Z. Zhao, Z. Xia and L. Dai, Nat. Nanotech., 2015, **10**, 444-452.

8 L. Ma, S. Chen, Z. Pei, Y. Huang, G. Liang, F. Mo, Q. Yang, J. Su, Y. Gao, J.A. Zapien and C. Zhi, ACS Nano, 2018, **12**, 1949-1958.

9 Y.-P. Deng, Y. Jiang, D. Luo, J. Fu, R. Liang, S. Cheng, Z. Bai, Y. Liu, W. Lei, L. Yang, J. Zhu and Z. Chen, ACS Energy Lett., 2017, **2**, 2706-2712.

10 Q. Wang, Y. Lei, Z. Chen, N. Wu, Y. Wang, B. Wang and Y. Wang, J. Mater. Chem. A, 2018, **6**, 516-526.

11 X. Li, F. Dong, N. Xu, T. Zhang, K. Li and J. Qiao, ACS Appl. Mater. Interfaces, 2018, **10**, 15591.
12 D. Bin, B. Yang, C. Li, Y. Liu, X. Zhang, Y. Wang and Y. Xia, ACS Appl. Mater. Interfaces, 2018, **10**, 26178.
13 H. Li, Q. Li, P. Wen, T. B. Williams, S. Adhikari, C. Dun, C. Lu, D. Itanze, L. Jiang, D. L. Carroll, G. L. Donati, P. M. Lundin, Y. Qiu and S. M. Geyer, Adv. Mater., 2018, **30**, 1705796.